CARBON 48 (2010) 2941–2947

available at www.sciencedirect.com

ScienceDirect

journal homepage: www.elsevier.com/locate/carbon

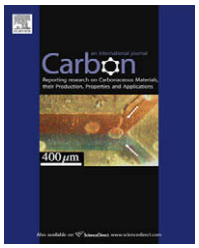

Selective removal of metallic single-walled carbon nanotubes by combined *in situ* and post-synthesis oxidation

*Bing Yu, Peng-Xiang Hou, Feng Li, Bilu Liu, Chang Liu *, Hui-Ming Cheng*

Shenyang National Laboratory for Materials Science, Institute of Metal Research, Chinese Academy of Sciences, 72 Wenhua Road,Shenyang 110016, China

ARTICLE INFO

Article history:
Received 19 February 2010
Accepted 15 April 2010
Available online 21 April 2010

ABSTRACT

A combined *in situ* and post-synthesis gas phase oxidation approach for selective removal of metallic single-walled carbon nanotubes (m-SWCNTs) is reported. The *in situ* oxidation is performed by introducing a small amount of oxygen during the synthesis of SWCNTs by floating catalyst chemical vapor deposition, and the post-synthesis oxidation is conducted by heat-treating the synthesized SWCNTs in air at 400 °C. A combination of characterization techniques shows that m-SWCNTs were selectively removed as a result of their higher reactive activity to oxygen compared to semiconducting SWCNTs, and the diameter distribution of the SWCNTs is narrowed to a range of 1.5–2.0 nm. The mechanism of the combined *in situ* and post-synthesis oxidation approach is discussed.

1. Introduction

Single-walled carbon nanotube (SWCNT) is one of the most promising materials for future electronics [1,2]. In particular, semiconducting SWCNTs (s-SWCNTs) are very attractive for making nanoscale electronic devices because of their small dimension, good chemical stability, and unique transport feature. A major obstacle to the application of SWCNTs in nanoelectronics is that almost all the current available synthesis techniques produce a mixture of s-SWCNTs and metallic SWCNTs (m-SWCNTs). Therefore, a protocol to obtain high purity s-SWCNTs is highly important. Several approaches for the enrichment of s-SWCNTs have been developed, such as solution-phase separation [3–5], electrical breakdown of m-SWCNTs [6,7], gas phase plasma treatment [8,9], light irradiation [10,11] and selective reaction/interaction [12–15]. Alternatively, selective surface growth of s-SWCNTs and m-SWCNTs were also reported recently, which are realized by selecting suitable carbon sources [16], *in situ* ultraviolet (UV) irradiation [17], and thermal annealing of the catalyst particles [18]. Although notable progresses have been made, shortcomings of complex operating procedure, additional unwanted contamination and un-scalability still need to be overcome. On the other hand, SWCNTs with large diameter (>1.5 nm) can provide sufficient band gaps that lead to high on/off ratio and enhanced mobility, and allow for good electrical contacts [19]. Therefore, SWCNTs with optimum diameter distribution are highly desired for assembling electronic devices. It will be appealing to develop an easy and scalable approach that can produce s-SWCNTs with optimum tube diameter, high purity and well-retained structural intactness.

Gas phase oxidation is a widely used method for purification of SWCNTs [20]. However, it usually does not function in enriching s- or m-SWCNTs due to the similar oxidation temperatures of amorphous carbon impurity and different types of SWCNTs. In this study, we propose a combined *in situ* and post-synthesis oxidation approach for selective removal of m-SWCNTs. The *in situ* oxidation is performed by introducing a small amount of oxygen during the synthesis of SWCNTs by floating catalyst chemical vapor deposition (FCCVD). The SWCNTs thus synthesized show two separated oxidation peaks as revealed by thermogravimetric analysis,

* *Corresponding author:* Fax: +86 24 2390 3126.
E-mail address: cliu@imr.ac.cn (C. Liu).
0008-6223/$ - see front matter
doi:10.1016/j.carbon.2010.04.032

which indicates a possibility for selective removing part of the SWCNTs by further oxidation. The post-synthesis oxidation is conducted by heating the as-synthesized SWCNTs at 400 °C for 5–10 h at ambient atmosphere. Thermogravimetric analysis revealed that one of the two original oxidation peaks disappeared while another one remained unchanged. Combinational characterizations show that the remained sample is s-SWCNTs dominated, and these s-SWCNTs have a narrow diameter distribution of 1.5–2.0 nm. The working mechanism of the combined *in situ* and post-synthesis oxidation approach is discussed.

2. Experimental

2.1. *In situ* oxidation of SWCNTs

The *in situ* oxidized SWCNTs were prepared by an oxygen-assisted FCCVD method at 1100 °C using CH_4 as carbon source. Briefly, 200 ml/min H_2 flowed through a quartz tube reactor with a diameter of 25 mm inserted into a horizontal tubular furnace. When the temperature of the reactor was increased to 1100 °C, a mixture of ferrocene/sulfur powder (the ratio of sulfur is 0.5 wt.%) put at the upstream of the reactor started to be sublimated and transported into the reaction zone by the H_2 gas flow. Then, 3 ml/min CH_4 and 0.2 ml/min O_2 flow was introduced into the reactor. The synthesis process lasted for 30 min. Finally, the reactor was cooled down to room temperature naturally. Membranaceous products were collected from the inner wall of the reactor. These *in situ* oxidized SWCNTs are denoted as IO-SWCNTs.

2.2. *Post-synthesis oxidation of SWCNTs*

The IO-SWCNTs film was put into a quartz tube with a diameter of 25 mm and a length of 1 m. The quartz tube was then inserted into a tubular furnace with both sides open for gas phase oxidation under ambient atmosphere. The oxidation was performed at 400 °C for a period of 5–10 h. The oxidized SWCNTs were further dipped in diluted hydrochloric acid to remove iron catalyst particles. The SWCNTs obtained by post-synthesis oxidation at 400 °C for 10 h is denoted as PO-SWCNTs.

2.3. *Characterizations*

The morphology of the SWCNT samples was characterized by scanning electron microscope (SEM, Nova NanoSEM 430) and high resolution transmission electron microscope (HRTEM, JEOL2010 at 200 kV and Tecnai G2 F30 at 300 kV). The thermal stability of the SWCNT samples was measured by a thermogravimetric analyzer (NETZSCH STA 449C). Laser Raman spectroscopy was used to investigate the variation of the signals of m- and s-SWCNTs [21–23]. The Raman spectra of the SWCNT samples were recorded using four different laser wavelengths of 785 nm (1.58 eV), 633 nm (1.96 eV), 514 nm (2.41 eV) and 488 nm (2.54 eV). Visible near-infrared (Vis/NIR) spectra (600–2500 nm) of the SWCNT samples were collected using a spectrophotometer (Varian Cary 5000 UV–Vis–NIR). Typically, 1 mg SWCNT sample was first ultrasonicated in 5 ml water with 1 wt.% sodium dodecyl sulfate (SDS). Then the suspension was filtered using a membrane filter with a pore diameter of 20 nm. The SWCNTs membrane was then transferred to a glass surface for the Vis/NIR characterizations.

3. Results and discussion

Fig. 1 shows the differential thermogravimetry (DTG) curve of the IO-SWCNTs synthesized by the oxygen-assisted FCCVD method (bottom one). Two distinct peaks centered at 460 and 530 °C can be clearly observed. This is quite different from the behavior of SWCNTs obtained without undergoing *in situ* oxidation (top one, denoted as OF-SWCNTs), where only one broad oxidation peak appears in the DTG plot. The distinctly separated oxidation peaks of the IO-SWCNTs indicate that it is possible to eliminate the SWCNTs with higher reactive activity to oxygen from the sample by post-synthesis oxidation. We can see from Fig. 1 that the IO-SWCNTs started to be oxidized at around 400 °C, thus the temperature of the post-synthesis oxidation was set to be 400 °C. And PO-SWCNTs were obtained by heat-treating the IO-SWCNTs at 400 °C for 10 h. The DTG curve of the PO-SWCNTs is also shown in Fig. 1 (middle one). Only one peak centered at 530 °C is observed for the PO-SWCNTs. The absence of the peak at 460 °C indicates that the SWCNTs with lower anti-oxidation capability have been removed by the post-synthesis oxidation.

The optical, SEM and TEM images of the PO-SWCNTs are shown in Fig. 2. The PO-SWCNTs are thin film-like, semi-transparent, and up to 5 cm^2 in area (Fig. 2a). SEM observations reveal that the PO-SWCNT film is composed of numerous entangled SWCNT bundles (Fig. 2b). Fig. 2c shows a typical HRTEM image of the PO-SWCNTs, it can be seen that the SWCNTs are straight and free from impurities attached on the surface. To further reveal the selective oxidation process, we also performed post-synthesis oxidation at 400 °C for 5 h. And the HRTEM image of thus obtained SWCNTs (denoted as PO5-SWCNTs) is shown in Fig. 2d. It can be seen that some SWCNTs become discontinuous and collapsed (as indicated by red arrows), while some other tubes still keep their tubular structure even in the same bundle. These results further verified that some SWCNTs are selectively etched during the oxidation treatment.

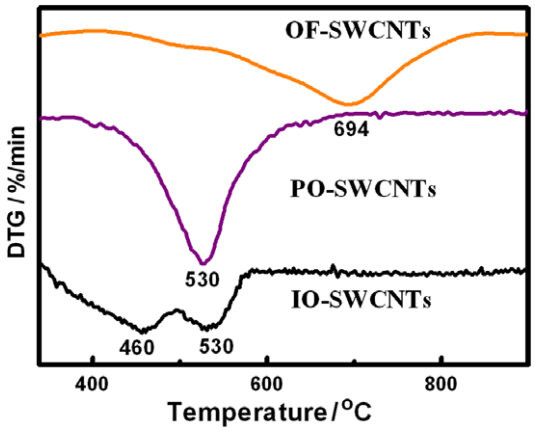

Fig. 1 – DTG curves of the IO-, PO- and OF-SWCNTs.

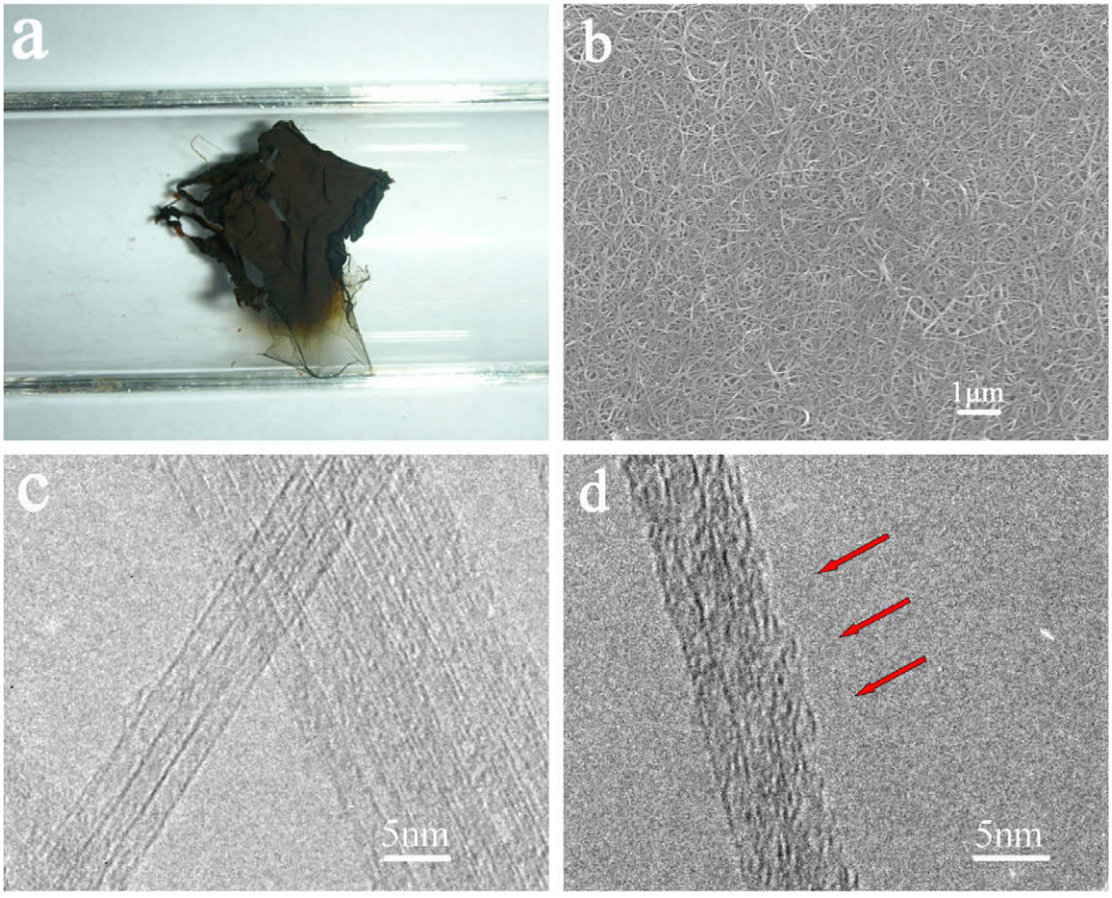

Fig. 2 – Optical (a), SEM (b), and TEM (c) images of the PO-SWCNTs, and (d) is a TEM image of the PO5-SWCNT sample.

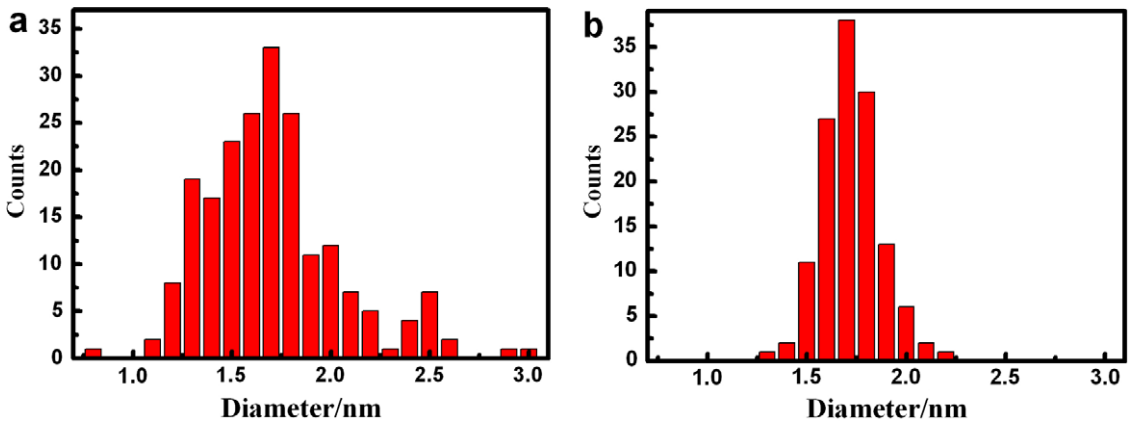

Fig. 3 – Histograms of diameter distributions of the IO-SWCNTs (a) and PO-SWCNTs (b) based on TEM observations.

The diameters of about 200 SWCNTs for each sample were measured under TEM, and the resultant histogram of diameter distribution for the IO- and PO-SWCNT is plotted in Fig. 3. The diameters of the IO-SWCNTs are distributed in a wide range of 0.8–3.0 nm, while that of the PO-SWCNTs are in the range of 1.5–2.0 nm. Obviously, SWCNTs with large and small diameters are both preferentially etched during the post-synthesis oxidation. Generally, SWCNTs with small diameters have high oxidation reactivity due to their large curvature [24], and the removal of the SWCNTs with diameters in the range of 2.0–3.0 nm may be ascribed to their higher content of defects compared to the nanotubes with smaller diameters.

The results of thermogravimetric analysis and electron microscopy observations indicate that a part of SWCNTs is selectively removed from the PO-SWCNT sample. It is important to reveal whether the remained SWCNTs are s-SWCNT or m-SWCNT dominated. The radial breathing mode (RBM) and G band features of laser Raman spectra can be used to assign and distinguish s- and m-SWCNTs, especially when

multiple excitation wavelengths are employed. Fig. 4 shows comparatively the radial breathing mode (RBM) of laser Raman spectra for the SWCNT samples with excitation wavelength of 633 nm (a), 514 nm (b), 488 nm (c), and 785 nm (d). The metallic (M) and semiconducting (S) features of the SWCNTs are indicated by dotted rectangles, as determined from the revised Kataura plot [25]. As shown in Fig. 4a, the signals appear at 175–230 cm^{-1} are originated from m-SWCNTs, while the signals at 115–170 cm^{-1} are from s-SWCNTs. The first metallic transition (M_{11}) are attributed to the first von Hove electronic transition of m-SWCNTs with diameters of 1.07–1.37 nm (ω_{RBM} (cm^{-1}) = 223.5/d_t (nm) + 12.5) [12,26]. In addition, the third and fourth semiconducting (S_{33}, S_{44}) transitions are attributed to the third and fourth von Hove electronic transition of s-SWCNTs with diameters of 1.47–2.19 nm. Interestingly, the M_{11} band from the PO5-SWCNTs is dramatically weakened, and that from the PO-SWCNTs is completely removed. This result strongly indicates that m-SWCNTs are preferential eliminated and that the etching process is mild since an intermediate state is observed, which is in accordance with the TEM observation shown in Fig. 2d. In Fig. 4b, compared with the IO-SWCNTs, the intensity of M_{22} band of the PO-SWCNTs turns weaker, while those of the S_{33} and S_{44} bands become stronger. In Fig. 4c, we can see that m- and s-SWCNTs co-exist in the IO-SWCNTs. However, the M_{22} bands of the PO-SWCNTs almost disappeared. In Fig. 4d, the signals of m-SWCNTs are dramatically weakened, and the signals of small diameter s-SWCNTs disappear, while the signals of large diameter s-SWCNTs are almost unchanged for the PO-SWCNTs. These above results indicate that the m-SWCNTs are effectively removed by the combined *in situ* and post-synthesis oxidations.

The above point is also evidenced by the tangential mode Raman spectra of the SWCNTs as shown in Fig. 5. The intensity ratios of G/D bands (Fig. 5a) for the IO-, PO5-, and PO-SWCNTs are ~8, 22, and 30, respectively, which indicates that amorphous carbon and SWCNTs with structural defects are gradually removed during the oxidation. The remained SWCNTs are in high purity and possess relatively intact structure. This coincides well with the result of HRTEM observations. In addition, comparison on the line shape of the G bands of the SWCNT samples further confirmed the selective removal of m-SWCNTs. As shown in Fig. 5b, the G band of the IO-SWCNTs is fitted with four semiconducting Lorentzian lines (centered at 1541, 1560, 1570 and 1590 cm^{-1}) and two broad, asymmetric metallic Breit–Wigner–Fano (BWF) lines (1515 and 1605 cm^{-1}) [27]. However, these two BWF peaks completely disappeared and the semiconducting peaks almost remain unchanged for the PO-SWCNTs (Fig. 5c).

Vis/NIR spectra can provide valuable information on the overall metallicity of SWCNTs, which cannot be obtained practically from resonant Raman data [28–31]. In accordance with the tight-binding model, the absorption peaks are attributed to electronic transitions of E_{11}^S, E_{22}^S and E_{11}^M between pairs of van Hove singularities in the density of states of s- and m-SWCNTs [12]. The optical absorption spectra of the IO- and

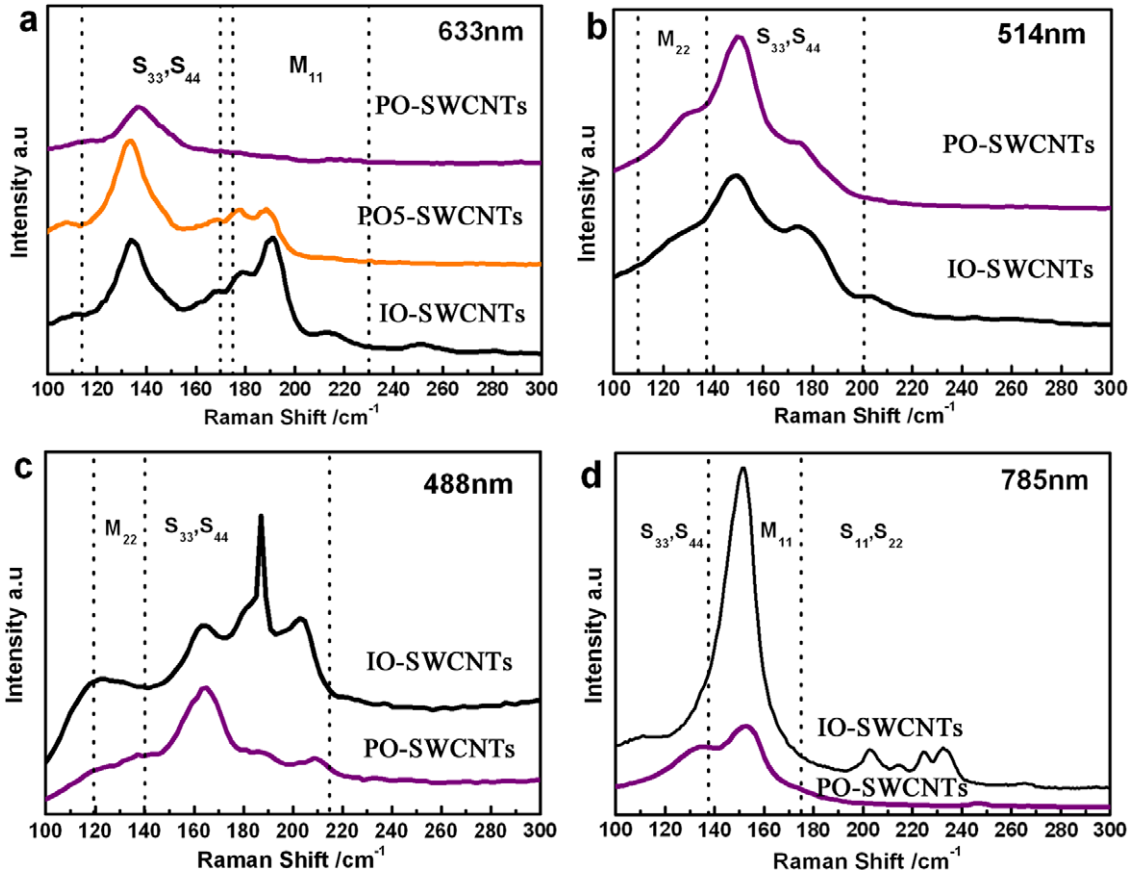

Fig. 4 – The resonant Raman spectra of the SWCNTs with excitation laser wavelengths of 633 (a), 514 (b), 488 (c), and 785 nm (d).

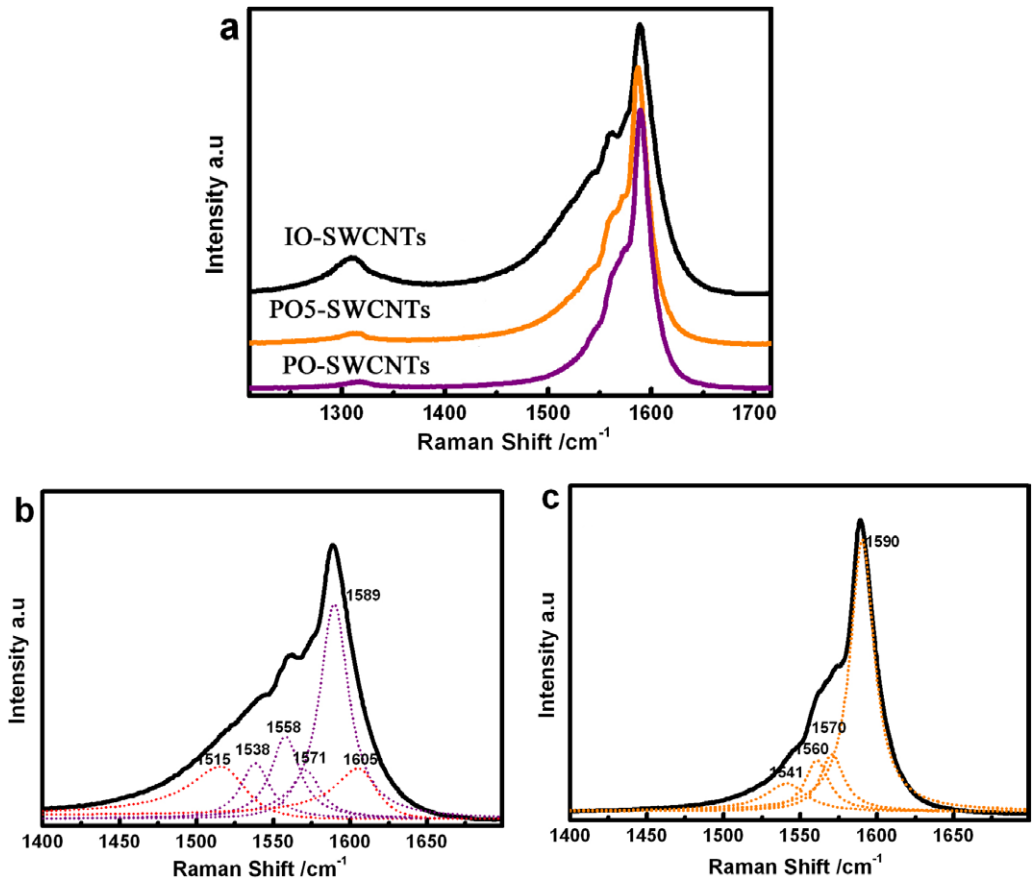

Fig. 5 – G and D mode of the resonant Raman spectra of the SWCNT samples with excitation wavelength of 633 nm (a). Curve fitting of G band of the IO-SWCNTs, four semiconducting Lorentzian line shapes and two metallic BWF line shapes (red color) can be observed (b). Curve fitting of G band of the PO-SWCNTs, only four semiconducting Lorentzian line shapes are identified (c). (For interpretation of the references in colour in this figure legend, the reader is referred to the web version of this article.)

PO-SWCNTs were recorded and shown comparatively in Fig. 6. For the IO-SWCNTs, the s-SWCNTs related bands (S_{11} and S_{22}) can be observed near 1200 nm (S_{11}) and 2200 nm (S_{22}), and the m-SWCNTs related bands (M_{11}) are observed near 880 nm. The absorption bands of S_{11}, S_{22} and M_{11} presumably represent the absorption bands of individual, micelle-isolated nanotubes [32]. The broad curve suggests that the samples contain small nanotube bundles. It can be seen that the M_{11} transition peak almost disappeared for the PO-SWCNTs. Whereas the intensities of the S_{11} and S_{22} peak only decreases slightly, suggesting that the majority of m-SWCNTs are removed by the post-synthesis oxidation. Therefore, the results of the absorption spectra substantially accord well with the results of laser Raman characterization discussed above.

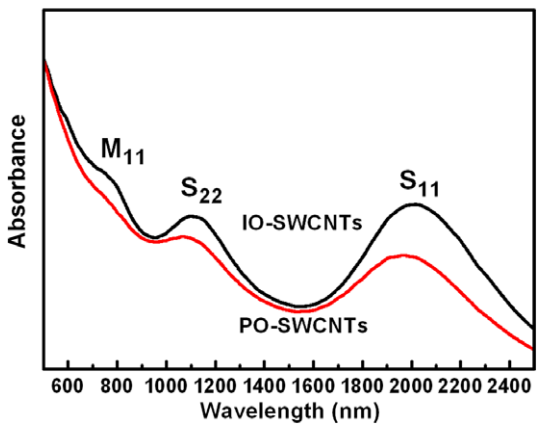

Fig. 6 – Vis/NIR spectra of the IO- and PO-SWCNTs.

Therefore, an enrichment of s-SWCNTs with a narrow diameter distribution (1.5–2.0 nm) is realized by our combined *in situ* and post-synthesis oxidation approach. The working mechanism of the *in situ* and post-synthesis oxidations is discussed as follows. When small amount of oxygen is introduced during the synthesis of SWCNTs by FCCVD method, the oxygen will preferentially attack and etch amorphous carbon and highly defective SWCNTs which have a poor anti-oxidation capability. Actually, these impurity and defective nanotubes usually co-exist with SWCNTs for normal SWCNT samples (without *in situ* oxidation treatment), and they may ignite neighboring SWCNTs when being oxidized. Therefore, SWCNT samples usually show one broad oxidation peak in their thermogravimetric analysis. The function of the *in situ* oxidation in this study is to remove these impurities and as a result, two separated oxidation peaks are shown in the DTG plot of the IO-SWCNTs. Because the amount of

introduced oxygen for *in situ* oxidation is very limited (otherwise large amount of SWCNTs will be burned off), a post-synthesis oxidation is needed to enrich the s-SWCNTs and to narrow its diameter distribution. It has been reported that m-SWCNTs are more easily to be etched than for s-SWCNTs, for example by plasma-etching [8], light irradiation [10,11], and oxidation [33]. In this study, our results of post-synthesis oxidation confirm that m-SWCNTs are preferentially oxidized while s-SWCNTs are well-retained. The DTG peaks centered at 460 and 530 °C shown in Fig. 1 are mainly responsible for the oxidation of m-SWCNTs and s-SWCNTs, respectively. On the other hand, SWCNTs with small radius of curvature have higher strain in the C–C bonding configuration [24], and SWCNTs with large diameters (>2 nm) may contain more structural defects, especially for those synthesized by CVD method at relative low temperatures. Therefore, SWCNTs with small [8] and large diameters are largely eliminated by the post-synthesis oxidation treatment.

4. Conclusions

In summary, a combined *in situ* and post-synthesis oxidation method is proposed for enriching s-SWCNTs with a narrow diameter distribution by preferentially eliminating m-SWCNTs and s-SWCNTs with small/large diameters. The s-SWCNTs with well-preserved structure are obtained in large-scale and their diameters are mostly distributed in the range of 1.5–2.0 nm. This combined *in situ* and post-synthesis oxidation approach shows advantages of large-scale, high efficiency, low cost, environment-friendliness, and simultaneous selectivity on the diameter and electrical property of SWCNTs. The resultant SWCNTs with desirable transport property and tube diameter will be promising for fabricating CNT-based electronic devices.

Acknowledgements

We thank Ms. Xi Ling and Prof. Zhang Jin for help in 514 and 785 nm Raman measurements. The authors also thank Mr. Dai-Ming Tang for the TEM characterizations. This work was financially supported by MOST of China (2006CB932701, 2008DFA51400), NSFC (90606008, 50672103, 50921004), and Chinese Academy of Sciences.

Appendix A. Supplementary data

Supplementary data associated with this article can be found, in the online version, at doi:10.1016/j.carbon.2010.04.032.

REFERENCES

[1] Martel R, Schmidt T, Shea HR, Hertel T, Avouris P. Single- and multi-wall carbon nanotube field-effect transistors. Appl Phys Lett 1998;73(17):2447–9.
[2] Tans SJ, Verschueren ARM, Dekker C. Room-temperature transistor based on a single carbon nanotube. Nature 1998;393(6680):49–52.
[3] Zheng M, Jagota A, Strano MS, Santos AP, Barone P, Chou SG, et al. Structure-based carbon nanotube sorting by sequence-dependent DNA assembly. Science 2003;302(5650):1545–8.
[4] Arnold MS, Green AA, Hulvat JF, Stupp SI, Hersam MC. Sorting carbon nanotubes by electronic structure using density differentiation. Nat Nanotechnol 2006;1(1):60–5.
[5] Tanaka T, Jin H, Miyata Y, Fujii S, Suga H, Naitoh Y, et al. Simple and scalable gel-based separation of metallic and semiconducting carbon nanotubes. Nano Lett 2009;9(4):1497–500.
[6] Collins PC, Arnold MS, Avouris P. Engineering carbon nanotubes and nanotube circuits using electrical breakdown. Science 2001;292(5517):706–9.
[7] Seidel R, Graham AP, Unger E, Duesberg GS, Liebau M, Steinhoegl W, et al. High-current nanotube transistors. Nano Lett 2004;4(5):831–4.
[8] Zhang GY, Qi PF, Wang XR, Lu YR, Li XL, Tu R, et al. Selective etching of metallic carbon nanotubes by gas-phase reaction. Science 2006;314(5801):974–7.
[9] Zheng G, Li QQ, Jiang KL, Zhang XB, Chen J, Ren Z, et al. Transition of single-walled carbon nanotubes from metallic to semiconducting in field-effect transistors by hydrogen plasma treatment. Nano Lett 2007;7(6):1622–5.
[10] Huang HJ, Maruyama R, Noda K, Kajiura H, Kadono K. Preferential destruction of metallic single-walled carbon nanotubes by laser irradiation. J Phys Chem B 2006;110(14):7316–20.
[11] Zhang YY, Zhang Y, Xian XJ, Zhang J, Liu ZF. Sorting out semiconducting single-walled carbon nanotube arrays by preferential destruction of metallic tubes using xenon-lamp irradiation. J Phys Chem C 2008;112(10):3849–56.
[12] Strano MS, Dyke CA, Usrey ML, Barone PW, Allen MJ, Shan HW, et al. Electronic structure control of single-walled carbon nanotube functionalization. Science 2003;301(5639):1519–22.
[13] An L, Fu QA, Lu CG, Liu J. A simple chemical route to selectively eliminate metallic carbon nanotubes in nanotube network devices. J Am Chem Soc 2004;126(34):10520–1.
[14] Balasubramanian K, Sordan R, Burghard M, Kern K. A selective electrochemical approach to carbon nanotube field-effect transistors. Nano Lett 2004;4(5):827–30.
[15] An KH, Park JS, Yang CM, Jeong SY, Lim SC, Kang C, et al. A diameter-selective attack of metallic carbon nanotubes by nitronium ions. J Am Chem Soc 2005;127(14):5196–203.
[16] Ding L, Tselev A, Wang JY, Yuan DN, Chu HB, McNicholas TP, et al. Selective growth of well-aligned semiconducting single-walled carbon nanotubes. Nano Lett 2009;9(2):800–5.
[17] Hong G, Zhang B, Peng B, Zhang J, Choi W, Choi J, et al. Direct growth of semiconducting single-walled carbon nanotube array. J Am Chem Soc 2009;131(41):14642–3.
[18] Harutyunyan AR, Chen G, Paronyan TM, Pigos EM, Kuznetsov OA, et al. Preferential growth of single-walled carbon nanotubes with metallic conductivity. Science 2009;326(5949):116–20.
[19] Kim W, Javey A, Tu R, Cao J, Wang Q, Dai HJ. Electrical contacts to carbon nanotubes down to 1 nm in diameter. Appl Phys Lett 2005;87(17):173101.
[20] Hou PX, Liu C, Cheng HM. Purification of carbon nanotubes. Carbon 2008;46(15):2003–25.
[21] Jorio A, Saito R, Hafner JH, Lieber CM, Hunter M, McClure T, et al. Structural (n, m) determination of isolated single-wall carbon nanotubes by resonant Raman scattering. Phys Rev Lett 2001;86(6):1118–21.
[22] Dresselhaus MS, Dresselhaus G, Jorio A, Souza AG, Saito R. Raman spectroscopy on isolated single wall carbon nanotubes. Carbon 2002;40(12):2043–61.

[23] Fagan JA, Simpson JR, Landi BJ, Richter LJ, Mandelbaum I, Bajpai V, et al. Dielectric response of aligned semiconducting single-wall nanotubes. Phys Rev Lett 2007;98(14):147402.
[24] Zhou W, Ooi YH, Russo R, Papanek P, Luzzi DE, Fischer JE, et al. Structural characterization and diameter-dependent oxidative stability of single wall carbon nanotubes synthesized by the catalytic decomposition of CO. Chem Phys Lett 2001;350(1–2):6–14.
[25] Strano MS. Probing chiral selective reactions using a revised Kataura plot for the interpretation of single-walled carbon nanotube spectroscopy. J Am Chem Soc 2003;125(51):16148–53.
[26] Luo ZT, Pfefferle LD, Haller GL, Papadimitrakopoulos F. (n, m) Abundance evaluation of single-walled carbon nanotubes by fluorescence and absorption spectroscopy. J Am Chem Soc 2006;128(48):15511–6.
[27] Brown SDM, Jorio A, Corio P, Dresselhaus MS, Dresselhaus G, Saito R, et al. Origin of the Breit–Wigner–Fano lineshape of the tangential G-band feature of metallic carbon nanotubes. Phys Rev B 2001;63(15):155414–8.
[28] Lebedkin S, Hennrich F, Skipa T, Kappes MM. Near-infrared photoluminescence of single-walled carbon nanotubes prepared by the laser vaporization method. J Phys Chem B 2003;107(9):1949–56.
[29] Geng HZ, Lee DS, Kim KK, Han GH, Park HK, Lee YH. Absorption spectroscopy of surfactant-dispersed carbon nanotube film: modulation of electronic structures. Chem Phys Lett 2008;455(4–6):275–8.
[30] Wang RK, Park HO, Chen WC, Silvera-Batista C, Reeves RD, Butler JE, et al. Improving the effectiveness of interfacial trapping in removing single-walled carbon nanotube bundles. J Am Chem Soc 2008;130(44):14721–8.
[31] Kim WJ, Lee CY, O'brien KP, Plombon JJ, Blackwell JM, Strano MS. Connecting single molecule electrical measurements to ensemble spectroscopic properties for quantification of single-walled carbon nanotube separation. J Am Chem Soc 2009;131(9):3128–9.
[32] O'Connell MJ, Bachilo SM, Huffman CB, Moore VC, Strano MS, Haroz EH, et al. Band gap fluorescence from individual single-walled carbon nanotubes. Science 2002;297(5581):593–6.
[33] Qiu HX, Maeda Y, Akasaka T. Facile and scalable route for highly efficient enrichment of semiconducting single-walled carbon nanotubes. J Am Chem Soc 2009;131(45):16529–33.